Quaternary International xxx (xxxx) xxx–xxx

Contents lists available at ScienceDirect

Quaternary International

journal homepage: www.elsevier.com/locate/quaint

Recent avulsion history of Sefidrud, south west of the Caspian Sea

Safiyeh Haghani[a,*], Suzanne A.G. Leroy[b]

[a] Experimental Techniques Centre, Brunel University London, UK
[b] CEREGE, Aix-Marseille University, CNRS, IRD, Collège de France, Technopôle de L'Environnement Arbois-Méditerranée, BP80, Aix-en-Provence, 13545, France

ARTICLE INFO

Keywords:
Sediment core
Radiocarbon dating
Historical maps
Sea level change
Sedimentology

ABSTRACT

The Sefidrud, a river flowing into south west Caspian Sea, is prone to avulsion. Previous studies of the river delta support the idea that several major avulsions have occurred during the past few thousand years. During the most recent major avulsion, a 23 km shift occurred along the coast. However, in literature the timing of the event is subject to uncertainty and therefore the causes of the avulsion remain unclear. Lying in the most populated area in Iran explains the importance to investigate the Sefidrud river avulsion. In this study, an 11 m-long sequence was obtained from an area where the river splits off into an old and a new distributary, and where a large pre-avulsion wetland had developed. Palaeo-environmental studies including sedimentology, macro-remain, and palynology were performed to detect changes in environment. Five radiocarbon dates were obtained to determine the avulsion age. In parallel an analysis of historical maps around the timing of the supposed avulsion and for more recent times provided a complementary way of refining the avulsion age. The results from this novel multidisciplinary study show that the last major avulsion occurred at a date after the early1800s and before 1929, during a period of rapid water level fall. Hence this is several centuries more recent than so far suggested. Studying aerial photographs, this research confirms the occurrence of minor avulsion between 1955 and 2014 where the avulsion point is around 2 Km from the coast line, and during a period of sea level fall. The results of this study also suggest that beyond the immediate effects on society and agriculture, avulsion increases the rate of coastal erosion near the abandoned distributary, as sediments are temporarily sequestered on the floodplain and causes intensive erosion. Avulsion has also major impact on coastal lagoons and inland wetlands by river diverting into the lagoons and wetlands.

1. Introduction

Avulsion is a process characteristic to channelised depositional systems, where channels aggrade or prograde faster than surrounding non-channelised adjacent areas. This drives formation of new channels, redistributing water flow and bedload through the new system. Avulsion is controlled by intrabasinal processes such as river meandering and delta lobe switching, and extrabasinal processes such as climate, tectonic and sea level (base-level) change (Stouthamer and Berendsen, 2007). Increasing sediment load or water volume due to climate change influences avulsion (Wells and Dorr, 1987). Tectonic movement causes avulsion by its effect on floodplain gradients and changes in river courses (Jones and Schumm, 2009) and the probability of avulsion increases as a consequence of subsidence (Stouthamer and Berendsen, 2007). Sea level rise and fall cause avulsion by influencing the aggradation rate in the overbank or floodplain areas (regional aggradation rate) and within the channel (local aggradation rate) (Aslan and Autin, 1999; Aslan et al., 2005). The regional and local aggradation rates are influenced by tectonic movements, changes in base-level, discharge and sediment load. Furthermore, human activities, including channel diversion for irrigation through artificial and natural levee breaks and channel blockages, may trigger a river avulsion (Heyvaert and Baeteman, 2008).

Avulsions can be abrupt or gradual and often have catastrophic consequences for nearby populations (Slingerland and Smith, 2004). For instance avulsion of the Yellow River in China in 1855 CE occurred overnight (Slingerland and Smith, 2004), while avulsions in the Meuse-Rhine River in Europe often required several centuries to complete, with durations of up to 1250 years (Stouthamer and Berendsen, 2000). Beyond the immediate effects on population and agriculture, even further downstream near to river mouth, coastal erosion may increase dramatically as sediment supply may be cut off for hundreds of years (Haghani and Leroy, 2016; Kakroodi et al., 2013; Slingerland and Smith, 2004). This has been shown for example in coastal area near to Amir-Abad (Fig. 1B) where the coastal erosion increased significantly as a result of avulsion (Haghani and Leroy, 2016). Documenting past

* Corresponding author.
E-mail addresses: safiyeh.haghani@brunel.ac.uk, Safiyeh.Haghani@gmail.com (S. Haghani).

https://doi.org/10.1016/j.quaint.2018.06.034
Received 19 December 2017; Received in revised form 30 April 2018; Accepted 21 June 2018

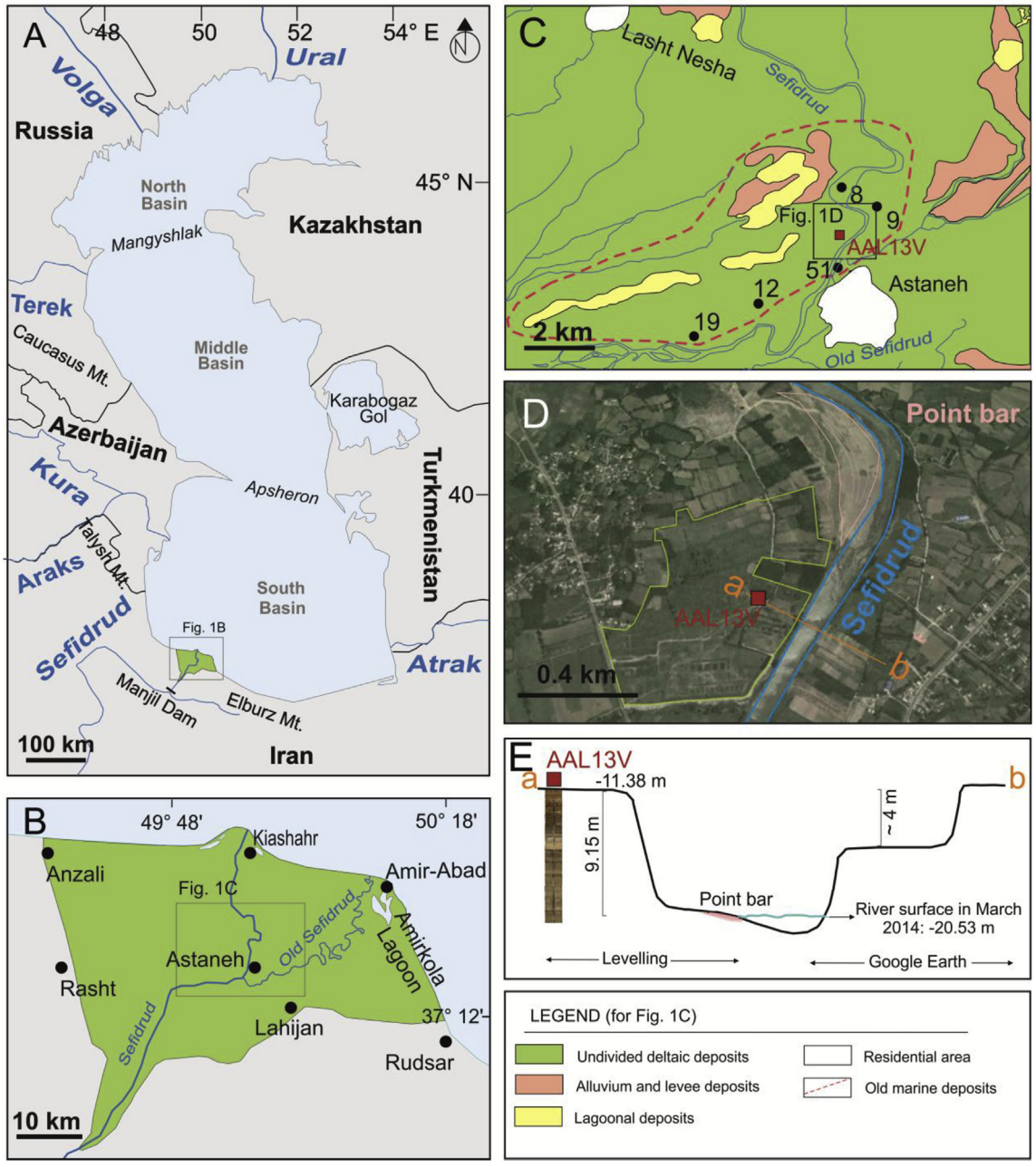

Fig. 1. A: Caspian Sea, B: Study area (SW of Caspian Sea), C: Location of core AAL13V (red square). Fine sediment deposition near Astaneh (black circles) with core numbers from Kazancı and Gulbabazadeh (2013). Flow direction of small rivers is from SW to NE. Source of this geological map is from the Geological Survey of Iran 1/100 000 Rasht, series sheet 5964 compiled by Khabaznia and Sadeghi (2004). D: Location of AAL13V in Google Earth Map. Pink crescent-shaped features represent present-day point bars and the green line shows the boundary of marsh area. E: Cross section of Sefidrud north of Astaneh Town area (Profile a-b in Fig. 1D). (For interpretation of the references to colour in this figure legend, the reader is referred to the Web version of this article.)

avulsions, finding the causes of avulsion, and interpreting processes are essential to mitigate the impact of possible future avulsions, such as the loss of agricultural land and flooding severity increase (Jotheri et al., 2016; Mahmood and Ullah, 2016). It may also contribute to forecast future avulsions; however, this is very difficult (Chakraborty et al., 2010).

The present paper focuses on avulsion in the delta of the Sefidrud, a river flowing into the south-west of the Caspian Sea (Fig. 1A). The Caspian Sea has no outlets, and in consequence loses water only through evaporation. The Caspian Sea has experienced a severe drop up to c. 3 m followed by a sharp rise in the 20th century, with speeds up to hundred times larger in scale than the current oceanic rate (Fig. 3, Kaplin and Selivanov, 1995). The rivers flowing from high mountains (that are located in the south-west and west of the Caspian Sea) such as the Sefidrud and the Kura (Fig. 1A) are the main sources of sediment supply to the Caspian Sea. As a consequence of the Caspian's isolation, it has experienced many very rapid water level fluctuations. The changes in water level have affected the lives of nearby inhabitants since ancient times in many different ways, including avulsions (Dolotov and Kaplin, 2005; Haghani et al., 2016a; Kosarev, 2005; Kroonenberg et al., 2007; Leroy et al., 2010; Naderi Beni et al., 2013a; Rucevska et al., 2006).

Around the Caspian Sea, avulsions have been recorded in the Kura River (Hoogendoorn et al., 2005; Ollivier et al., 2016) and the Volga River (Overeem et al., 2003) during the Little Ice Age. The Kura River diverted its course between 1600 CE and 1800 (Hoogendoorn et al., 2005), when the river split into two branches a few kilometres away

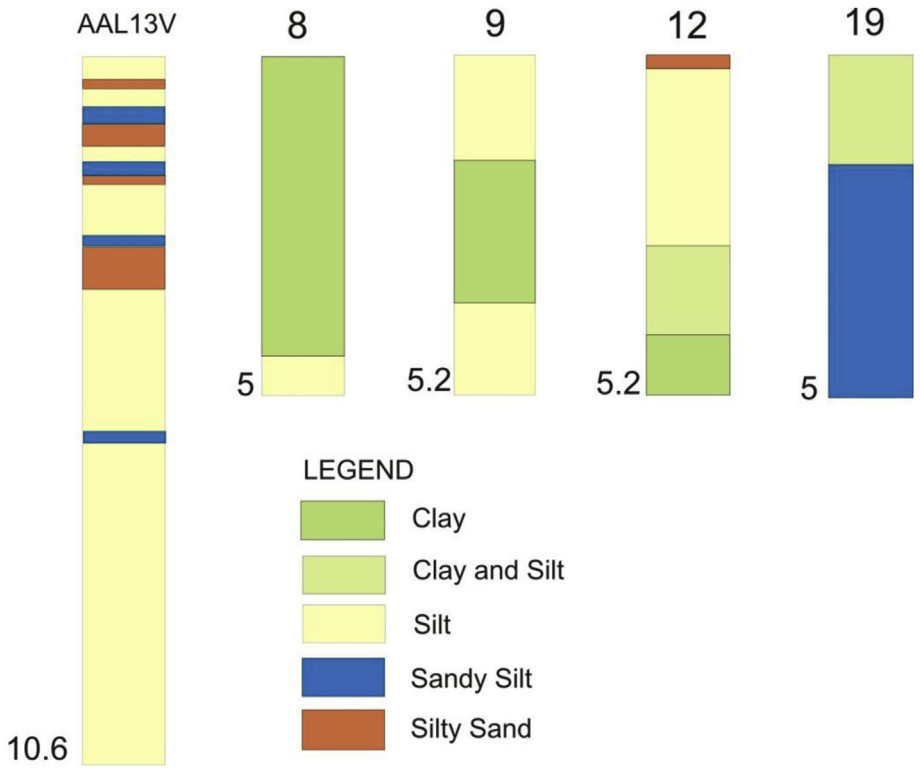

Fig. 2. Cores containing fine sediments from this study (AAL13V) and Kazancı and Gulbabazadeh, 2013 (cores 8,9,12,18).

from the mouth known as the Navigable Kura (after avulsion) and the Old Kura (Pre avulsion river). Almost the entire runoff is now concentrated in the Navigable Kura, while the Old Kura dies out (Kosarev and Kostianoy, 2005). In the case of the Sefidrud, the river has repeatedly changed its course through the area between Anzali and Amir-Abad separated by 65 km (Fig. 1B) (Kousari, 1986); and the last main avulsion occurred when the river diverted its course from the east, near Amir-Abad, towards the west near Kiashahr, shifting its outlet c. 23 km westwards (Fig. 1B). A literature review indicates that evidence for the date of the avulsion is elusive; nevertheless, this has not prevented specific and seemingly precise dates from being cited in various publications. The most commonly cited date is around 1600 CE (Kazancı and Gulbabazadeh, 2013; Krasnozhon et al., 1999; Lahijani et al., 2009; Leroy et al., 2011; Naderi Beni et al., 2013b); however, the timing evidence of this major event has so far remained unclear and unsupported by published radiocarbon dates or any other document. In this investigation, we aim to address the timing of occurrence and the main causes of the avulsion by using both a sediment core multiproxy investigation and a re-analysis of old maps.

2. Study area

The Caspian Sea extends zonally from 46.6 to 54.8° East and meridionally from 36.6 to 47.0° North (Fig. 1A). It is the largest lake on earth. It is fed by 130 rivers, the most significant being the Volga, which enters from the north and accounts for about 80 percent of the inflowing waters. Over 60% of the area is shallower than 100 m, with the depth increasing towards the south, reaching a maximum of 1025 m

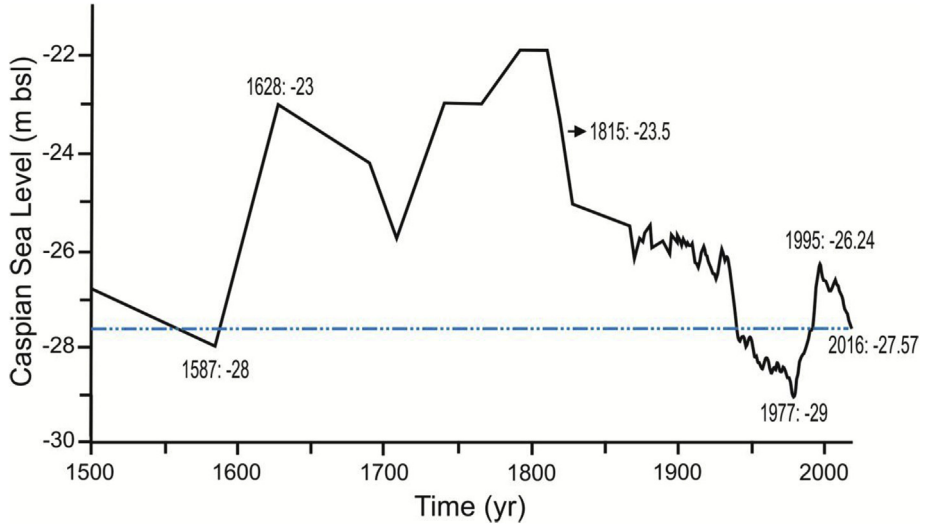

Fig. 3. Caspian Sea level; 1500 to 1900 from Naderi Beni et al. (2013a); 1900 to 1992 from Lepeshevkov et al. (1981); 1992 to May 2016 from USDA (2016).

Table 1
Radiocarbon dates of the samples from the AAL13V sequence. Calibrated ages in AD are reported for 2σ range with probabilities shown in parentheses. Dates from ANSTO (OZR) and Queen's University Belfast (UBA).

Laboratory number	Sample ID	Depth (cm)	Material Type	^{14}C Age (yr BP)	F^{14}C	Calibrated yr AD (2σ range)	Median Probability
OZR388	AAL2-46-48	142	Rootlets	modern	1.2584 ± 0.0100	1979–1983 (87.7%) 1961–1962 (10.2%) 1959 (1.7%) 1984 (0.4%)	c. 1981
UBA-29892	AAL5-52-53	430	Rootlets	65 ± 35	0.9920 ± 0.0043	1809–1926 (74.1%) 1689-1730 (25.2%) 1955 (0.6%)	c. 1868
UBA-32548	AAL6-5-6	480	Bulk organic	132 ± 23	0.9837 ± 0.0028	1800–1891 (45.8%) 1677-1765 (37.3%) 1908–1940 (15.9%)	1823
OZR389	AAL7-15-17	589	Rootlets	200 ± 40	–	1723-1816 (52.1%) 1642- 1697 (26.9%) 1916–1950 (16%) 1834–1878 (4.9%)	1769
UBA-22974	AAL10-90	956	Root/Branch	1900 ± 30	0.7893 ± 0.0030	50-179 (93.1%) 187- 213 (5.1%) 29- 38 (1.8%)	103

(Boomer et al., 2005) (Fig. 1A). The current water level is at 27.57 m bsl. The Sefidrud (the white river) is located in the south west of the Caspian Sea (Fig. 1B) The Sefidrud delta consists of Palaeocene to Quaternary intertwined marine and floodplain deposits. Abundant distributary channels, local swamps and wetlands are common features in the area. The population density within the delta is very high and a considerable part of the delta in cultivated and covered by rice paddies and tea farms. The pre avulsion river is known as the Old Sefidrud and post avulsion as the Sefidrud (or New Sefidrud). Prior to the last major avulsion, the Old Sefidrud occupied a single, well-developed north-eastward flowing channel, bypassing the Amirkola Lagoon (Fig. 1B). Thereafter, at a point south west of Astaneh town (Fig. 1B), the river began to avulse northward. Through a network of newly created and pre-existing channels, the avulsed flow eventually entered the Caspian Sea near Kiashahr town (Fig. 1B). As a result of avulsion, the Old Sefidrud became considerably shallower due to avulsive sedimentation; but nowadays it still retains a channel flowing to the Caspian Sea. After avulsion, the Sefidrud is a northward-flowing meandering channel with an average water depth of ~2.5 m and a width between 250 and 400 m (Krasnozhon et al., 1999). Kousari (1986) indicated that this meandering pattern is a result of river reaching to the basement surface of the Caspian Sea. According to logs of sediment cores described in Kazancı and Gulbabazadeh (2013), the deposition of dark grey to black fine-grained sediments, sometimes only laminated, north of Astaneh Town was observed on at least 5 m thickness in four locations (Figs. 1C and 2). Deposition of these fine sediments could be related to an old wetland environment, which we call here the Astaneh wetland. The geological map, from Geological Survey of Iran, north and west of Astaneh Town singles out the occurrence of lagoonal deposits, alluvium and levee deposits in what is otherwise termed loosely undivided deltaic deposits (Khabbaz-nia and Sadeghi, 2004) (Fig. 1C). This evidence combined with the previous cores taken in the Astaneh wetland (Kazancı and Gulbabazadeh, 2013) and our field observation suggests that the wetland area covered at least 4 by 12 km (Fig. 1 C). These sequences of fine sediment are often capped by coarser sediment (silty sediment or silty sand in cores 9 and 12 respectively), indicating that the relatively large Astaneh wetland disappeared progressively. To examine the hypothesis of presence of a buried wetland and to estimate the age of the last major avulsion of the Sefidrud, two sediment cores were taken from an area covered by floodplain sediments at north of Astaneh Town and close to the current Sefidrud (Fig. 1C).

2.1. Water and sediment discharge regime

The Manjil Dam was built across the Sefidrud in 1962, around 50 km upstream from the avulsion node. The lake created behind the dam has altered flow conditions in the breakout area. Downstream from the dam, suspended loads are high, which may indicate that channels in the breakout area might be degrading. Since 1962, most of the sediment load that was deposited in the breakout area is now trapped in the lake. Due to the high rate of sediment load, by 1978, 40% of the capacity of the dam reservoir was full. As a result, flushing operations were operated between 1980 and 1998. Only during winter flushing period of 1984–1985, 135 million tonnes of sediments were flushed downstream, whereas, normal condition (*e.g.* for the rest of the year) sediment discharge was as low as 9.8 million tonnes (Haghani et al., 2016b). Table 2 shows typical post-dam sediment and water discharges for the period of 1980–1998. Since 1998 the flushing operations have been suspended due to climate variations and increasing periods of drought in Iran

Table 2
Flushing operation statistics from 1980 to 1998, Water Research Institute, Ministry of Energy, Iran as in Yamani et al. (2013).

Flushing period	Sediment Discharge (10^6 t)		Water Discharge (10^6 m^3)	
	Flushing period	Normal condition (the rest of the year)	Flushing period	Normal condition (the rest of the year)
1980–1981	21.30	9.90	536	4926
1981–1982	10.30	3.8	390	3154
1982–1983	48.80	14.8	1513	4365
1983–1984	72.50	12.2	1017	3747
1984–1985	135.30	9.8	1606	4564
1985–1986	43.80	5.90	1084	3019
1986–1987	31.60	5.60	978	2902
1987–1988	59.10	35.30	1812	6577
1988–1989	55.20	4.70	1057	2636
1989–1990	31.9	1.50	681	2827
1990–1991	23.3	3.20	664	2473
1991–1992	18.6	9.30	664	4796
1992–1993	22.2	6.90	605	3996
1993–1994	52.9	5	2321	5447
1994–1995	46.1	7.70	2136	4489
1995–1996	12.5	10.30	812	4703
1996–1997	15.9	2.10	867	1815
1997–1998	11	3.40	374	3823

(Yamani et al., 2013). The constructed dam has significantly altered the flooding regime.

2.2. Climate, modern vegetation

Because of its great meridional extension, the Caspian Sea overlaps several climatic zones. The northern coastal region has a continental climate with cold winters and hot summers, the middle part is characterised by mild winters and hot summers, while the southern coastal region has a sub-tropical climate with mild winters and warm humid summers. The coastal zones of the northern and eastern Caspian Sea are mostly arid with average annual precipitation ranging between 100 and 300 mm. The western coast is semi-arid while the southern and southwestern coasts are humid, receiving between 400 and 1200 mm of rain per year (Rucevska et al., 2006). Generally, precipitation decreases from west to east. The climate conditions largely influence the land use in the coastal region.

The coastline of the Caspian Sea is 7000 km long and varied. The northern and eastern parts of the Caspian coast encompass the Caspian Lowland desert with sand dunes, salt deserts and clay deserts. Vegetation is sparse and often dominated by salt-tolerant plants forming shrubs. The southern Caspian coastal zone consists of narrow, but lush, lowlands, locked in between the sea to the north and the Elburz Mountains to the south.

Deciduous forests, *i.e.* the Hyrcanian forest, have developed in the two mountain ranges (*i.e.* Elburz and Talysh Mountains), even including refugial areas for some past European species (Leroy and Roiron, 1996). The lowland coastal areas are almost entirely cultivated and few natural habitats are preserved in small nature parks protected for example by the Ramsar Convention. Agricultural activities in the north and east of the Caspian Sea are dominated by pastures, while the proportion of land used for crop production increases in the south and southwest. Additional crop production is found in areas where local water supply is plentiful such as in the vicinity of the rivers Volga, Terek and Sulak (Russia), Samur and Kura (Azerbaijan), Ural (Kazakhstan) and Sefidrud (Iran).

3. Material and methods

3.1. Coring

Coring took place north of Astaneh Town (Fig. 1C) in 2013 using a percussion corer in the area of the fine deposits highlighted by Kazancı and Gulbabazadeh (2013) (Fig. 2) and at 190 m from the current Sefidrud course, and c. 3700 m from the area where the Old Sefidrud splits off from the New Sefidrud. The coring location was located amongst agricultural fields but at the edge of an area that was unused, probably because it was too wet for agriculture (Fig. 1D). No obvious signs of ploughing, cropping or grazing were observed. Two parallel cores (AAL13V A and B, 1063 and 1026 cm), with offset 1 m long sections, were retrieved in order to obtain a continuous sequence. These offset core sections were aimed to cover gaps between the sections; but due to good coverage of core A, core B was only used to check the boundary between facies. Sedimentological analysis (including grain size and LOI analysis), ^{14}C dating, macrofossil analysis and palynological study were performed on section A that represents well the sequence AAL13V.

The coring location had higher elevation than the river surface and also the other bank of the river. Therefore, the accurate elevation was surveyed using a Leica Sprinter 150 M Electronic Level in March 2014 (*i.e.* 14 months after the coring campaign).

3.2. Sedimentology and radiocarbon dating

Magnetic susceptibility (MS) was measured using a Bartington MS2C core logging sensor at 2 cm intervals. The grain-size distribution was measured using laser diffraction (CILAS 1180). Ultrasonic pre-treatment ensured an adequate homogenization of the sample as well as a good dispersion of the suspension. Granulometric data were then processed using the GRADISTAT program and the sand–silt–clay triangular diagram suggested by Folk (1974) was used for naming textural group of the sediments. In addition, three-dimensional (3D) plot of grain-size data was performed using MATLAB software version 7.1. Sediment colour was determined using a Munsell Colour Chart.

Organic matter (OM) and calcium carbonate ($CaCO_3$) were estimated on 28 samples through loss on ignition, following Heiri et al. (2001). A total of five radiocarbon dates were obtained at the Chrono Centre, Queen's University Belfast and Australian Nuclear Science and Technology Organisation (ANSTO): three on rootlets, one on a root or branch and one additional date on bulk sediment (Table 1). Due to lack of appropriate material for radiocarbon dating and due to the occurrence of radiocarbon plateaux in the last centuries, five samples were selected for radiocarbon dating as follows: four from roots or small branches and one from bulk organic matter. To validate the four radiocarbon dates that were obtained from woods, in-situ bulk organic matter from the 481-479 cm depth organic-rich layer was selected for radiocarbon dating. A radiocarbon age younger than 1950 CE (modern ages) was calibrated using the CALIBomb programme (Reimer et al., 2004) with the Northern Hemisphere zone 2 calibration dataset (Hua et al., 2013). The dates older than 1950 CE were calibrated using the CALIB programme version 7.1 (Stuiver and Reimer, 1993) with the IntCal13 calibration curve (Reimer et al., 2013). Calibrated ages were reported for 2σ range with probabilities, in Table 1. However, median age was used to calculate the sedimentation rate. The age-depth model was produced using the software CLAM with linear interpolation (Blaauw, 2010).

3.3. Macro–remains

Following Birks (2001), seventeen samples with a weight of 15–20 g from the sequence were deflocculated using 10% tetra-sodium pyrophosphate solution. The samples were then washed through a column of sieves with a mesh diameter of 500, 125 and 53 μm. The residue from each sieve was studied using a stereo-microscope (magnifications up to 90 ×). All the fractions were scanned, but only the samples above 500 μm were counted. The results are presented in percentage diagrams using the psimpoll software, version 4.27 (Bennett, 2007). A zonation by CONISS after square-root transformation of the percentages data was applied.

3.4. Palynology

Fifteen samples of a volume of 0.5–2 ml were analysed. The treatment consisted of an initial deflocculation with sodium pyrophosphate. Then, the samples were treated with cold hydrochloric acid (10%), cold hydrofluoric acid (32%), followed by a repeated cold hydrochloric acid treatment. After that, the samples were sieved through 120 and 10 μm meshes. Finally, the residues were mounted on glass slides in glycerol. The initial addition of *Lycopodium* tablets allowed the estimation of concentrations (in number of palynomorphs per ml of wet sediment).

A light microscope at ×400 magnification and at ×1000 for special identifications was used to count the palynomorphs. Pollen atlas and the reference collection at Brunel University London were used to identify the spores and pollen grains. Percentages were calculated on the terrestrial sum (average of 328 terrestrial pollen grains), and the diagrams were plotted using the psimpoll software. A zonation by cluster analysis (CONISS) after square root transformation was applied to the main terrestrial taxa.

3.5. Historical and recent maps

Historical documents available at Royal Geographical Society London have been consulted to confirm the timing of the avulsion

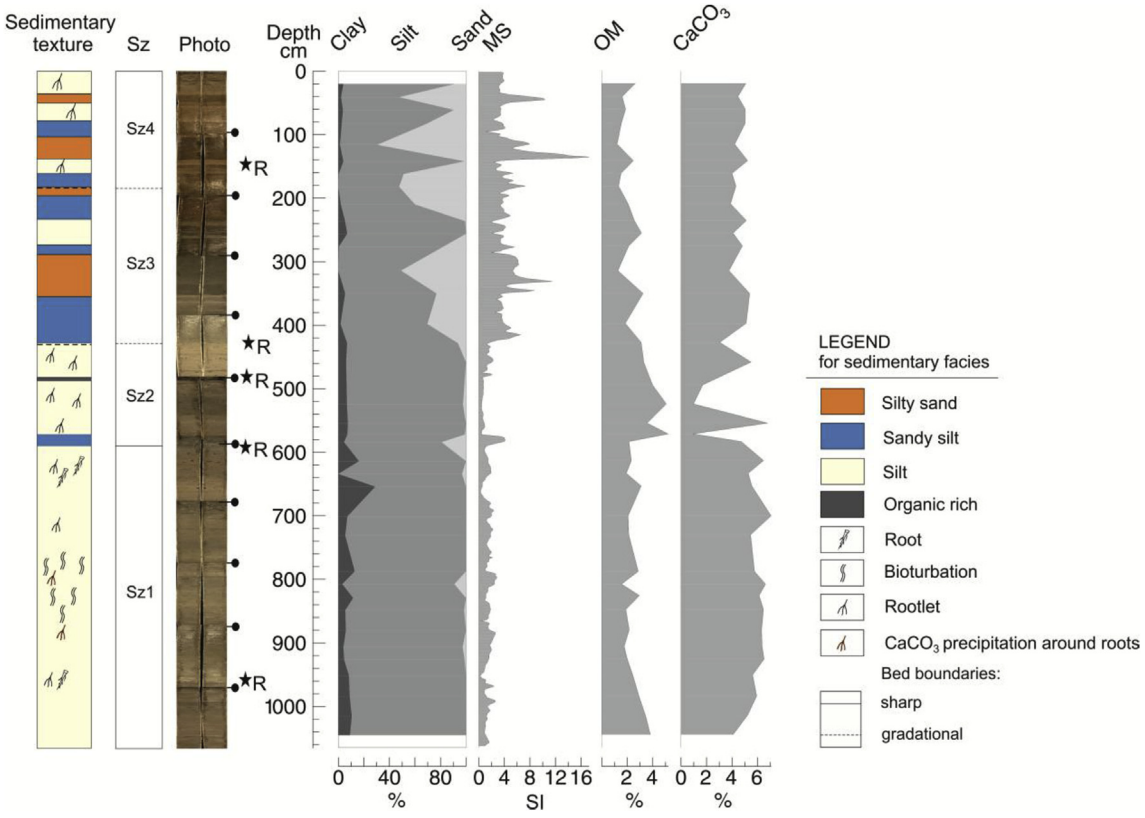

Fig. 4. Sedimentary sequence for Astaneh core AAL13V, displaying sedimentological zones (Sz), core photo, grain size (clay, silt and sand), magnetic susceptibility (MS), organic matter (OM) and calcium carbonate ($CaCO_3$) contents. The five black stars refer to the depths of the radiocarbon dates, and R: rootlets and roots (material dated). The black pin symbols refer to core section limits.

proposed by palaeo-environmental interpretation. However, these maps were only available to be consulted within the Royal Geographical Society, with no permission to take photo from the maps. Therefore, we were unable to include them in the publication. Aerial photographs of the year 1955, 1964, and 1982, also satellite images from Google Earth from 1991 to 2014 were used to identify minor recent avulsions.

4. Results

4.1. Last major avulsion

The cross section of the Sefidrud channel (a-b) is presented in Fig. 1E. Based on measurement, the elevation of coring location is −11.38 m bsl, which is 9.15 m higher than the river surface in March 2014 (*i.e.* −20.53 m). The elevation of the other side of the river was not precisely measured. However, based on the elevation provided by Google Earth, the clear height difference visually observed between the two river banks probably reached ~4 m (Fig. 1E).

4.1.1. Sedimentology and radiocarbon dating

The percentages of sand, silt and clay, also MS, OM % and $CaCO_3$% are presented in Figs. 4 and 5. Based on visual description, grain size and sedimentological analyses the sequence can be divided into four main sedimentological zones including:

Sz1, 1063-590 cm: dark greyish brown (10 YR 4/2) to brown (10 YR 4/3) and reddish brown (5 YR 4/3) silt occurs with rootlets and bioturbation at ~900-800 cm. The maximum amount of clay is observed in this zone and the following zone, *e.g.*, Sz2. The contacts within the beddings are gradual, except the sharp contact with the sandy silt from the next zone. Tree roots (~2 cm long and 0.4 cm wide) also were observed at the top of this zone in core A. Moreover, a large root (20 cm long and ~1 cm wide) was observed in core B, from 650 to 670 cm. The magnetic susceptibility is low in this zone, only up to three. The content of organic matter shows a slight decreasing trend in this zone with a background of ~2%. The carbonate contents have a background of 5%. A small maximum of clay (29%) is observed at 654 cm depth.

Sz2, 590-430 cm: medium bedded olive grey (5Y 4/2) sandy silt followed by thickly bedded reddish brown (5 YR 4/3) to brown (10 YR 4/3) silt with rootlets contain a very dark grey (10YR3/1) fine layer of organic rich silt in its middle (481–479 cm). The contact between organic matter layer and sandy silt is sharp, but it is gradual with the upper zone (Sz3). The content of organic matter shows a sudden increase at the base of this zone, reaching 5.2% at a 571 cm; this is followed by a slow decreasing trend upward. The calcium carbonate contents show abrupt fluctuations with two low points ~1% at the depths of 571 and 524 cm (Fig. 4).

Sz3, 430-184 cm: Alternation of grey (5Y 5/1) to dark grey (5Y 4/1) sandy silt, brown (10 YR 4/3) to grey (5Y 5/1) silty sand, and brown (10 YR 4/3) silt are observed. The magnetic susceptibility clearly shows higher values in this zone, even reaching ~11 at 331 cm. The content of organic matter and carbonate are lower and remain relatively constant towards the top.

Sz4, 184-0 cm: Alternations of brown (10 YR 4/3) silt with rootlets, and brown (10 YR 4/3) silty sand to sandy silt occur. The magnetic susceptibility is high and even reached ~18 at 135 cm. The content of organic matter and carbonate remain relatively constant towards the top.

In the absence of shells and seeds, the five radiocarbon dates were

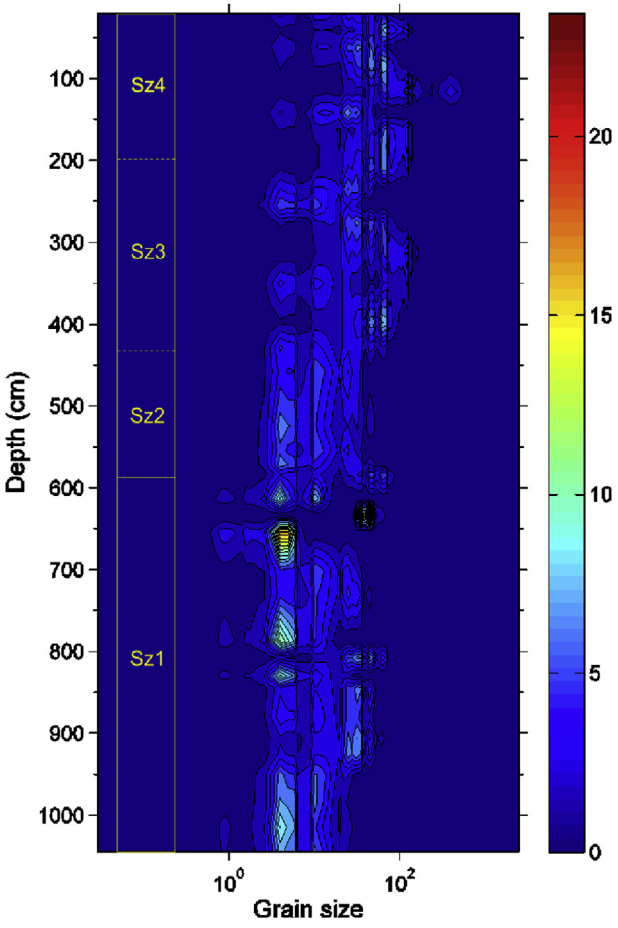

Fig. 5. 3D plot of grain size data in μm for the sequence AAL13V: the dark blue colour represents the lowest volume (%), while the red colour shows the highest volume (%). Sz: sedimentological zone. (For interpretation of the references to colour in this figure legend, the reader is referred to the Web version of this article.)

obtained from roots, rootlets and bulk organic materials at depths of 956, 589, 480, 430 and 142 cm along the sequence (Table 1). However, by selecting rootlets, a clear possibility of rootlet penetration into the soil/sediment exists and thus of obtaining slightly too young ages. Therefore, one sample was also selected from in-situ bulk organic matter at a depth of 480 cm, to validate the rest of the dates.

4.1.2. Macro–remains

Based on the results, the sequence is divided into three zones, as follows (Fig. 6):

Mz1, 1057–653 cm (8 samples): This zone is characterised by presence of $CaCO_3$ precipitation around the roots which reaches to 8.5% at a depth of 757 cm. Faecal pellets (up to 71%), clay flakes (up to 60%), plant material (up to 4.5%) and charcoal (2%) compose the rest of macro-remains.

Mz2, 653–401 cm (3 samples): This zone has a marked maximal amount of plant material (95%) at 567 cm. Small amounts of clay flakes and faecal pellets were observed.

Mz3, 401–26 cm (6 samples): This zone is marked by a maximal amount of clay flakes (up to 44%) and faecal pellets (71%). Furthermore, small amounts of plant materials and charcoal were also observed. This zone is similar to Mz1 but without the carbonate casts.

4.1.3. Palynology

Besides a rich sample at 663 cm depth, the concentrations were rather low. Four samples were barren: at 700, 615 and two in the upper 150 cm. Moreover, the palynomorphs were generally not well preserved. These two characteristics are typical for palynology in flood plain environments. Moreover extremely high values of fungal spores characterise the whole sequence.

In the arboreal pollen (AP), *Alnus* is clearly dominant. The other frequent tree pollens are *Quercus* and *Pterocarya,* the latter being an endemic genus (Mostajeran et al., 2016). In the non-arboreal pollen (NAP), the diagram is dominated by Amaranthaceae, Asteraceae, Poaceae and Cyperaceae pollen grains. Hardly any aquatic indicators occur, except in a few samples between 653 and 554 cm depth. Indicators of agricultural activities are found throughout the diagram. Based on the results, the sequence is divided to three zones (Fig. 7):

Pz1, from 1063 to 686 cm: *Alnus* is dominant (around 20%) with c. 5% of *Quercus* and of *Pterocarya*. *Pinus* and *Ephedra* are present. In the NAP, *Artemisia* and Amaranthaceae are dominant, with frequent Liguliflorae, Tubuliflorae and Poaceae. Reworked palynomorphs progressively increase.

Pz2, from 686 to 572 cm: *Pterocarya* values drop significantly across this zone. This zone is characterised by maximal aquatic pollen including: *Typha-Sparganium* (26% at 653 cm) and various fern spores, including *Azolla-Salvinia*. Cyperaceae increase up to 65% at 591 cm. A drop of reworked palynomorphs occurs. A pollen grain of *Tricolporopollenites sibiricum* was found at 653.5 cm depth (Wang and Harley, 2004.).

Pz3, from 572 to 236 cm: The percentages in this zone are highly variable due to wide changes in *Alnus* (4–78%) corresponding to opposite changes in Amaranthaceae. All the other trees drop to very low values. A general drop of *Artemisia* is observed. Liguliflorae and Tubuliflorae remain stable, as well as Poaceae. Fungal spores, including *Glomus* are very abundant. *Typha-Sparganium* is still abundant at the base of this zone.

4.2. Recent minor avulsions

Comparing aerial photographs from 1955 to 1964 (Fig. 8A and B) shows that a minor avulsion occurred during this period, where the avulsion point is around 2 Km from the coast line. Moreover, the Sefidrud direction changed westwards, in a period when sea level was relatively stable, but in an overall falling trend. Two coastal lagoons were formed in the west of the river as a result of avulsion, due to providing more sediment for sand barrier formation, hence development of lagoon behind it. Between 1964 and 1991 the active channel belt became narrower and multichannel, reflecting the impact of Manjil Dam construction in 1962, i.e. decrease of the sand fraction in the river load. A very minor avulsion occurred between these years (Fig. 8 B to D). Between 1991 and 2014, another minor avulsion happened and minor tributary became the main tributary (Fig. 8D and E). This corresponds to a period of overall water level fall. The latest avulsion had an impact on filling up the Kiashahr Lagoon more rapidly.

5. Interpretation

Based on different proxies (sedimentology, macro-remains and palynology), the sequence is subdivided into three main depositional environments presented in Fig. 9. Based on chronological data, the deposits record three stages of development and provide evidence for significant changes in sediment deposition.

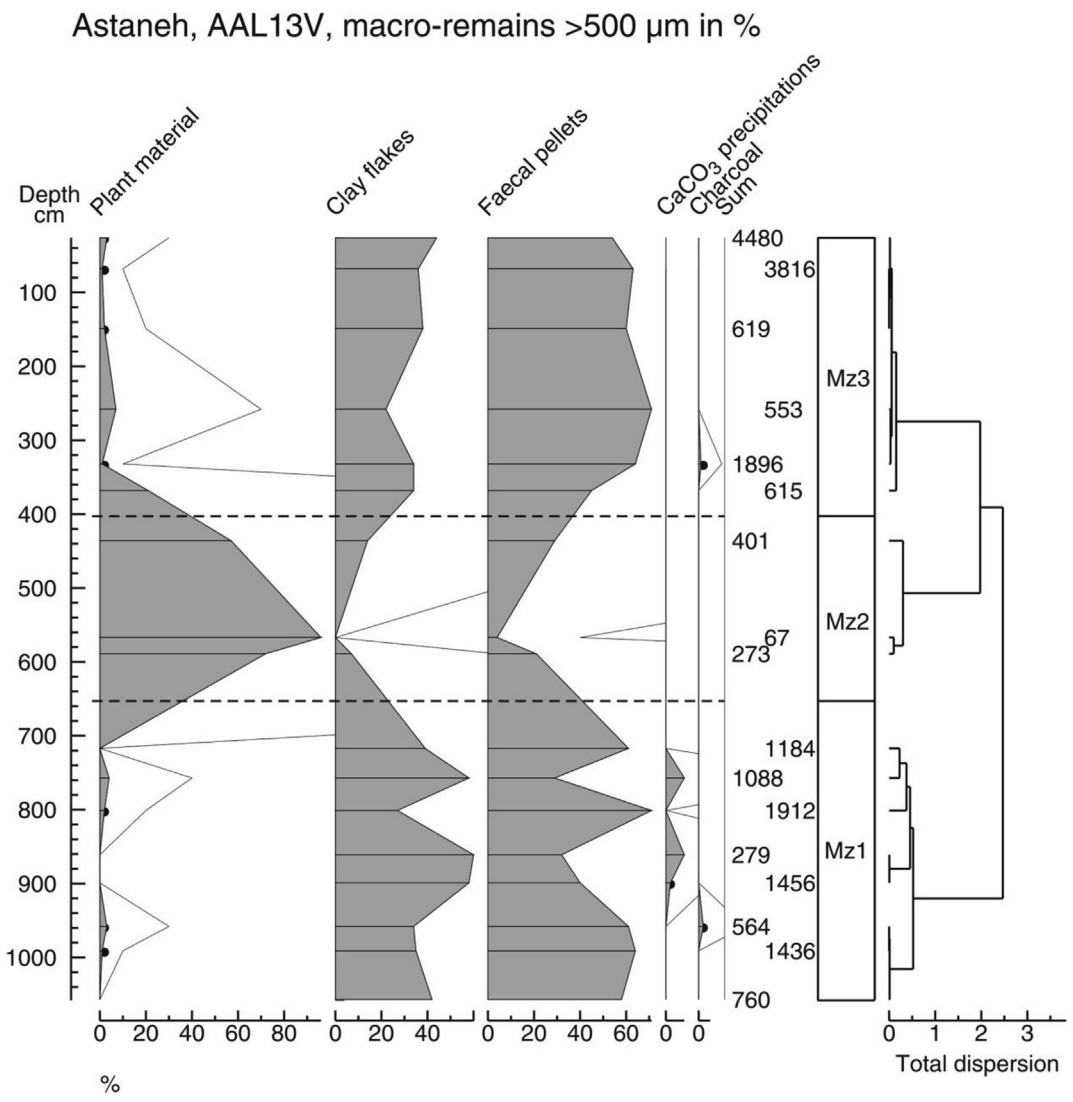

Fig. 6. Percentages of macro-remains above 500 µm. Black dots represent percentages below 1%.

5.1. Shallow water body (1063-430 cm)

The low magnetic susceptibility and relatively high amount of clay suggest a shallow water body environment (as shown also by the occurrence of *Spirogyra*, which requires shallow water for sporulation) surrounded by alder trees. This zone can be subdivided into two subzones.

5.1.1. Temporary shallow water body (1063-686 cm)

The lower part of zone I consist of horizontally-bedded dark greyish brown to reddish brown silt with rootlets and bioturbation (Sz1). This facies is characterised by low magnetic susceptibility. These fine grain sediments contain precipitation of $CaCO_3$ around rootlets, which suggests that the water body was temporary. Wieder and Yaalon (1982) indicated that carbonate precipitation is related to the metabolism of roots. High pressure of CO_2 as a result of root respiration contributes to a relatively rapid crystallisation of dissolved calcium.

5.1.2. Shallow water body with dense marshy vegetation (686-430 cm)

The top of Sz1 and the whole of Sz2 consist of dark greyish brown to reddish brown silt with in-situ tree roots and rootlets, and characterised by minimum magnetic susceptibility and maximum organic matter content (Fig. 4). The top of this zone has a maximal amount of plant material (Mz2 in macro-remain diagram and Sz2 with high amount of OM). The Cyperaceae (sedges) (Pz1) and the *Typha-Sparganium* (bulrushes and bur-reeds) (Pz2 and bottom of Pz3) are most likely from a local wetland and may make the bulk of the organic matter encountered in the sequence.

Most of these sediments (Zone I) were deposited as a part of a larger wetland (Fuchsia dashed line in Fig. 1C), *i.e.* the 'Astaneh Wetland' (Fig. 2). This wetland can only have developed in a quiet environment, possibly before the river avulsion. As the area is extensively faulted with many different distributary of the Sefidrud, the origin of the depression for the Astaneh wetland could be a sag pond created by collapse during tectonic movements, or an oxbow lake created due to river cut off.

5.2. Fluvial environment (430-184 cm)

The deposits consist of an alternation of reddish brown sandy silt and dark grey to olive brown silt. The sudden increase of MS and grain size shows an obvious change in depositional environment. Presence of

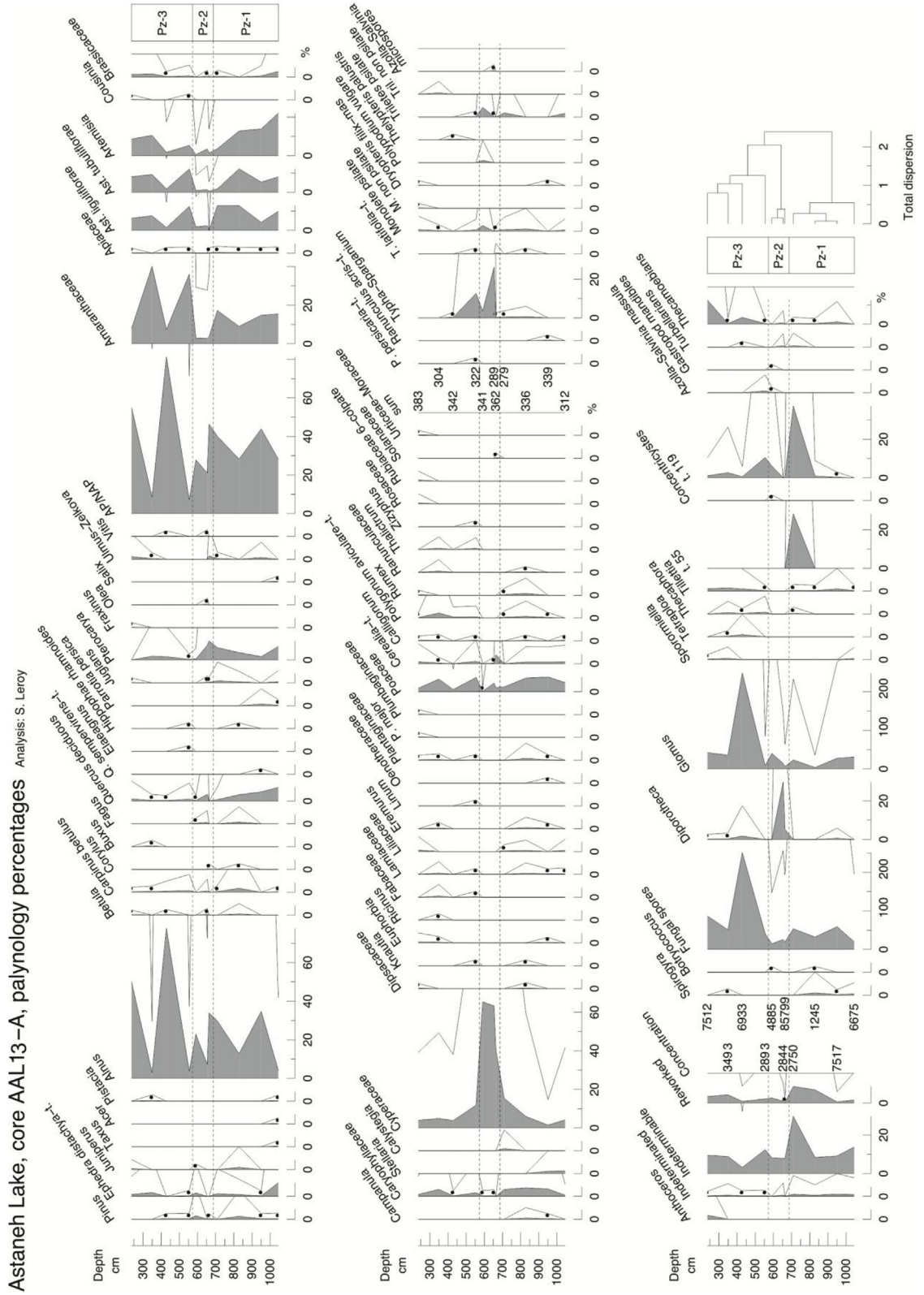

Fig. 7. Pollen, spores, non-pollen palynomorphs and dinocyst diagram in percentages for core AAL13-A. Black dot for values < 0.5%.

reworked pollen grains and fungal spores indicate erosion and suggest river transport. High MS in this zone could reflect a transport of minerals from igneous and metamorphic rock with an Elburz Mountains origin. Indeed, it is suggested that the channel deposits are linked to the avulsion of the Sefidrud. These fluvial deposits consist of point bar.

5.3. Marsh under river influence (184 cm to surface)

The upper sediments consist of alternating brown silt with rootlets, and brown silty sand to sandy silt. As the topmost date is very young, it indicates a sedimentation that has carried on until recently. This is perhaps linked to the progressive reduction of some contemporary

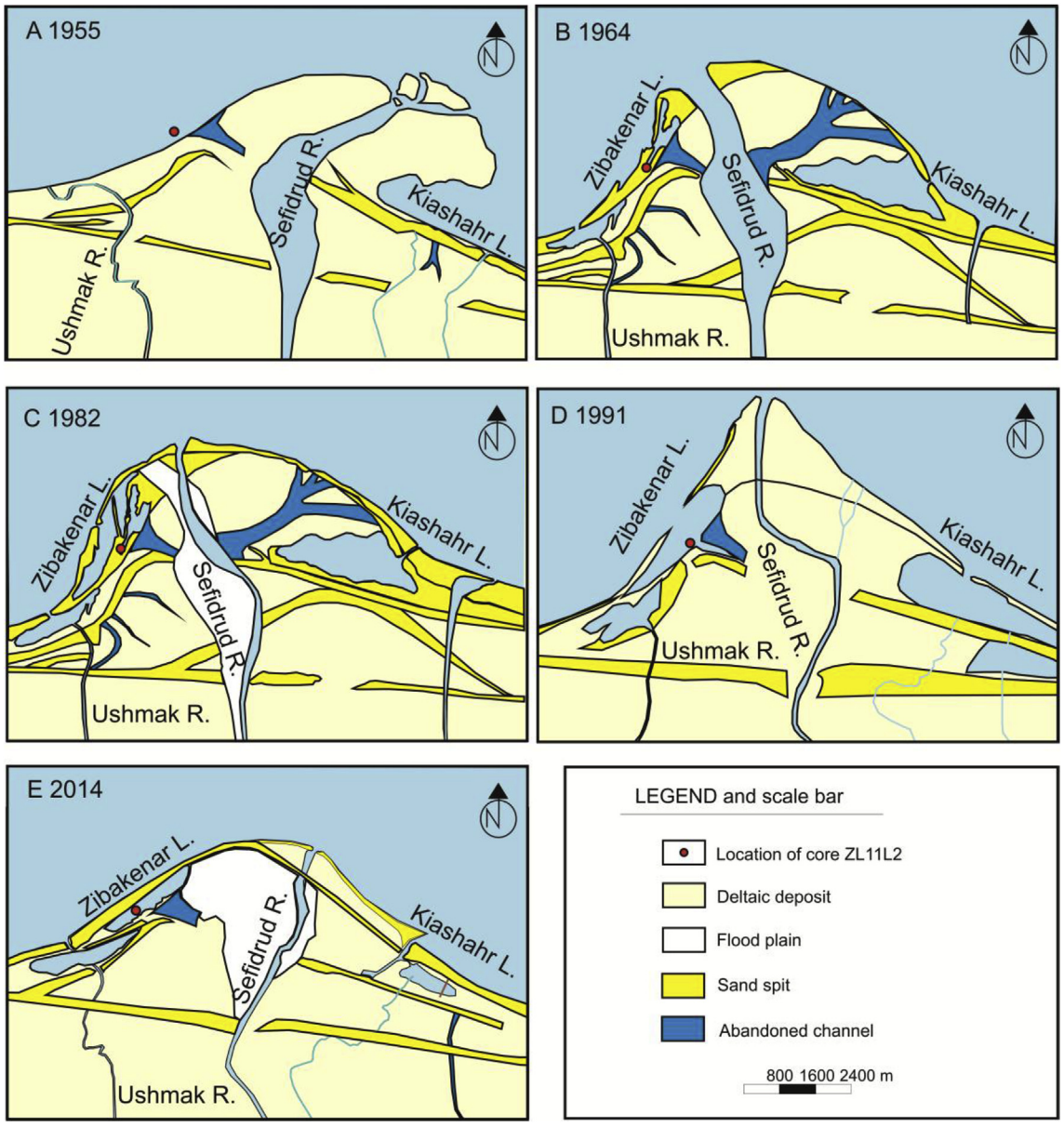

Fig. 8. Historical aerial photographs (A, B and C) and satellite image (D and E) from Sefidrud.

marshes, still visible at less than a km west of the coring location (the green line in Fig. 1D). High MS in the silty sand deposits suggests that the coarser fragments are deposited by river. This river is a small distributary of the Sefidrud that flows to the new seasonal wetland at a higher altitude than the Sefidrud (see Fig. 1C).

6. Discussion

6.1. Chronology and sedimentation rate

The chronology of the avulsion can be defined in two ways: firstly by the appearance of fluvial deposits in sequence AAL13V (start of facies II), and secondly from historical documents.

The age model indicates increasing sedimentation rates through the sequence, spanning from c. 100 CE to very recent years (Fig. 10). The oldest section of the sequence (956–589 cm and probably most of facies Ib) has the slowest sedimentation rate of 2.2 mm/yr. Sedimentation rate has increased in facies Ib to 5 mm/yr. Then the sedimentation rate increased to 25 mm/yr after avulsion (boundary between facies I and II), with a further increase to 43 mm/yr for the top facies. This suggests that after avulsion more sediment was deposited in the area.

The calibrated age for the radiocarbon date at 430 cm, which is located just below the boundary between facies I and II reflecting the avulsion, shows three probabilities. Based on the results (Table 1), avulsion is the most likely to have happened at a date between 1809 CE and 1926, with a 74.1% probability. Also, the event could have occurred at a date between 1680 CE–1730, with 25.2% probability. In both dating scenarios, facies II was deposited in an incised channel during rapid water level fall (Fig. 2). Indeed, incised channels mostly occur where rivers have eroded their delta plain as a result of sea level fall (Reading, 2009). During stages II and III, the Sefidrud has considerably cut into its flood plain; as now it is > 9 m lower than the surface of the current wetland (Fig. 1E). The pre-avulsion river, *i.e.* the Old Sefidrud, is still active, but at present the sedimentation is mainly

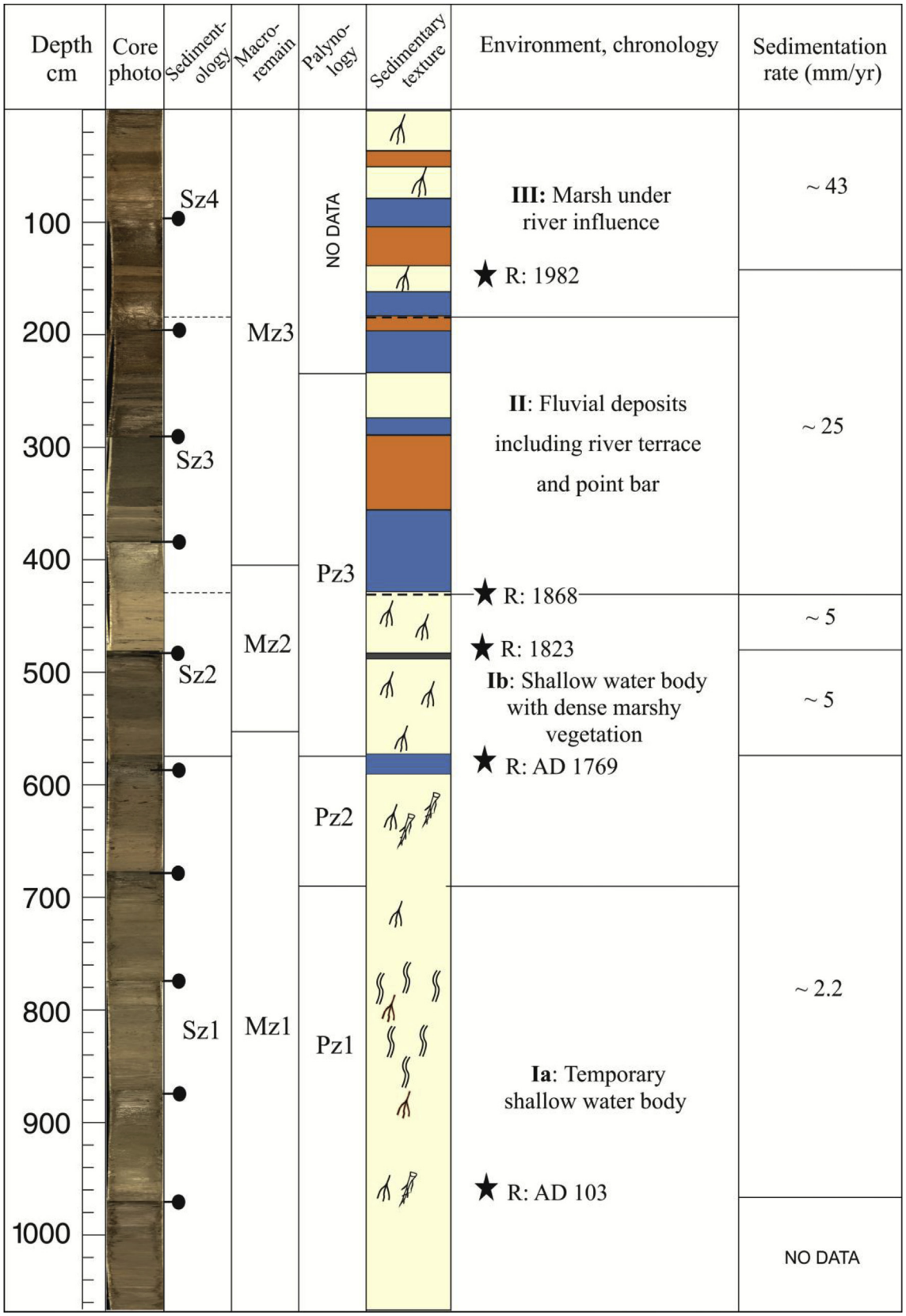

Fig. 9. Interpretation of facies based on sedimentology, macro-remains and palynology of the sequence of AAL13V. Black stars: radiocarbon dates. (See Fig. 3, for the legend for sedimentary facies).

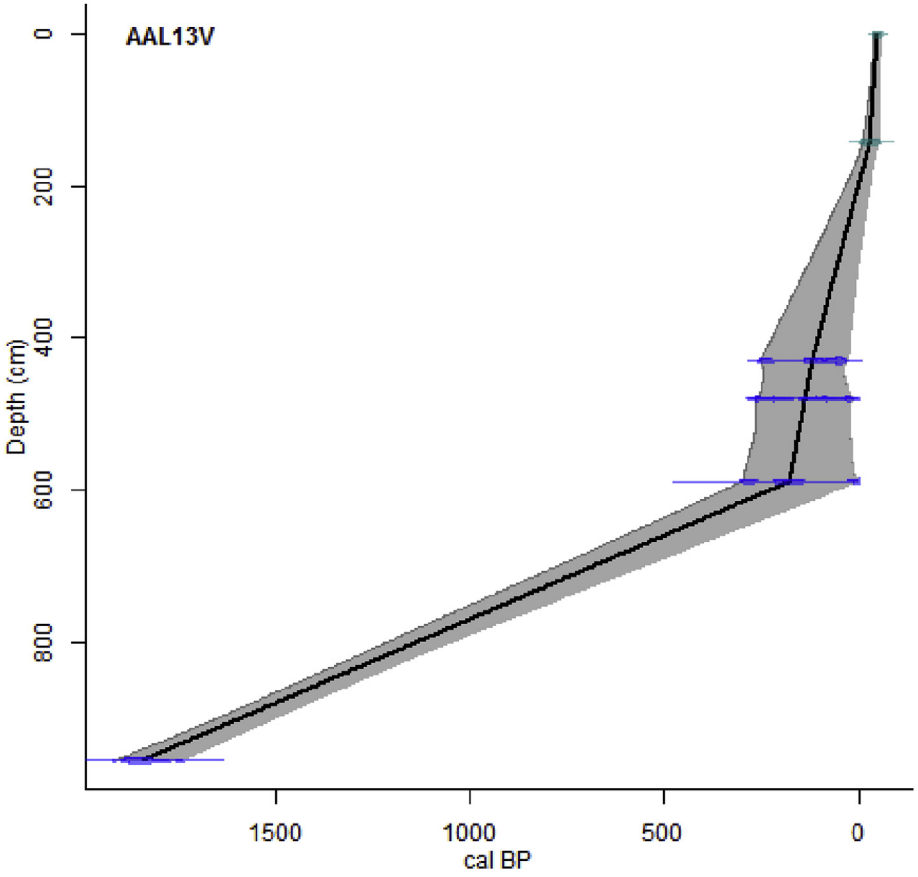

Fig. 10. Age depth modelling for the sequence produced by CLAM software using linear interpolation (Blaauw, 2010). Grey envelopes show 95% confidence intervals.

concentrated at the mouth of the New Sefidrud (Haghani et al., 2016b) and the main channel transports the bedload to the Caspian Sea. The new river delta began to infill the wetland near Astaneh Town and rapidly encroaching marsh vegetation as shown by a present detailed multidisciplinary analysis of one sequence that can however be put in the frame of a wider lithological survey of four other cores from Kazancı and Gulbabazadeh (2013) (Figs. 1C and 2). Virtually all levees and splays in the Old Sefidrud are now densely vegetated, and the channel is mostly active during high discharge events. A recent study showed that coastal erosion has increased abruptly in nearshore Old Sefidrud (Haghani and Leroy, 2016; Kakroodi et al., 2013), as sediment supply has decreased due to avulsion. Eventually, during the time the New Sefidrud is gradually evolving into a single meandering channel, as a part of the long-term tendency of the avulsion, probably similar to what have preceded in the past for the Old Sefidrud or for the Old Kura. The Astaneh wetland has nearly disappeared as a result of the Sefidrud diverting its course into the wetland. The same scenario happened for the coastal lagoons such as Kiashahr (Haghani et al., 2016b). These fluvial changes are hard to control and heavily impact a region that is fast developing. After the main avulsion, the area where the Old Sefidrud is flowing to the Caspian is subject to intensive erosion, as a result of abrupt reduction of sediment supply due to avulsion (Haghani and Leroy, 2016). Due to the inherent problems of radiocarbon dating in the last centuries (plateau), the most likely age of the avulsion derived from radiocarbon dating is between AD c. 1809 and c.1926.

The last map before avulsion was published in 1794 CE by Laurie and Whittle in A New Universal Atlas (A new map of the Persia, 1794). The first map after avulsion was a geological map published in 1957 CE based on surveys undertaken between 1927 and 1929. This map was published for the British Petroleum Company Limited by Edward Stanford Limited in London (Geological maps and sections of Persia, 1957).

Therefore this historical analysis based on well dated but discontinuous points and the sedimentological approaches based on a more continuous sequence but with more uncertainty in the dating have jointly much improved the timing previously based on speculative information (c. 1600 CE) by yielding solid data. Our investigation therefore provides accreditation to the timing of avulsion much after the sixteenth century – after 1794–1809 CE and indeed well into the 19th or the early parts of the 20th century – before AD -1926-1927. In brief the avulsion is at least 200 years, if not 300 years, younger than suggested in the literature.

6.2. *Causes and triggers*

The timing of both major and minor avulsions corresponds to a period of Caspian level fall. During the period of fall, longitudinal-profile adjustment forced by sea level fall, will start at the coastline and progresses landward by headward erosion resulting in knickpoint migration (Salter, 1993; Leeder and Stewart, 1996; Quirk, 1996). The point of intersection of the old and new graded longitudinal profile would put an upward limit on the stratigraphic effect of the sea-level fall (Leopold and Bull, 1979; Posamentier and Allen, 1993). Therefore, a drop in sea level is felt only several kilometres upstream for small, high-gradient rivers, whereas large, low-gradient rivers with larger drainage basins seem to adjust their profiles hundreds of kilometres

upstream (Blum and Toernqvist, 2000). For instance, in response to the last glaciation the small Obitsu River incised about 15 km upstream, the Colorado River nearly 100 km, and the Mississippi 300 km (Heijst and Postma, 2001). The morphologic concept of river-profile adjustment by headward erosion thus implies a time lag between the onset of a sea-level fall and the upstream adjustment of the river's longitudinal profile (Butcher, 1990). Therefore, the results from this research cannot confirm whether or not the sea-level fall had a role in avulsion. Experimental results from Heijst and Postma (2001) suggest that neither fall nor rise in sea level affects the upstream fluvial system, instantaneously.

By changing the water and sediment discharge patterns, Manjil Dam should be recognised as possible avulsion trigger. The dam and required flushing processes may lead the channel towards avulsion threshold by decreasing its ability to carry sediments and discharge and sudden increase of sediment load during the flushing period (Jones and Schumm, 2009).

Since the Sefidrud delta is heavily cultivated, channel diversion for irrigation through levee breaks and channel blockages should also be considered as avulsion trigger (Heyvaert and Baeteman, 2008).

7. Conclusions

The Sefidrud has avulsed repeatedly in the past few thousand years and this is an issue because its delta is one of the most intensively cultivated of Iran. The most recent major avulsion so far was thought to have occurred around 1600 CE, based on unsubstantiated information. We applied a two-pronged approach. Firstly, our radiocarbon data (of one sedimentary sequence with a detailed palaeoenvironmental study) suggest two different timing for the avulsion: (1) during 1680 CE–1730, with a low probability, (2) or more recently, between 1809 CE and 1926 with a higher probability. Secondly, the examination of historical maps is in agreement with the most recent date, and allows a higher level of precision: with a bracket between 1794 CE and 1929. This corresponds to a period of rapid Caspian Sea Level **fall**.

Aerial photographs confirm that Sefidrud has also experienced minor avulsions where avulsion point is around 2 Km to the coastline. These minor avulsions occurred between 1955 and 1964, and also between 1991 and 2014. These also correspond to a Caspian Sea-level fall. Manjil Dam should be recognised as possible avulsion trigger, due to changing the water and sediment discharge patterns. Finally, the channel diversion for irrigation purposes can be considered as avulsion trigger in the study area.

The results from this study in the frame of a set of sedimentary logs from the delta also revealed the presence of a buried wetland: the Astaneh wetland. This wetland has nearly disappeared as a result of the Sefidrud diverting its course in it. The same avulsion scenario is happening in other coastal lagoons in the area. Indeed, the minor avulsions, near to the shoreline, have strong impacts on the formation of coastal lagoons by providing more sediment for sand spit formation. The same process can lead to a progressive chocking of the lagoon, by decreasing its equilibrium. The other impact of avulsion is intensive erosion, as a result of abrupt reduction of sediment supply in the abandoned distributary mouth.

Appendix A. Supplementary data

Supplementary data related to this article can be found at http://dx.doi.org/10.1016/j.quaint.2018.06.034.

References

A new map of the Persia, 1794. Laurie and Whittle. London. .

Aslan, A., Autin, W.J., 1999. Evolution of the Holocene Mississippi River floodplain, Ferriday, Louisiana: insights on the origin of fine-grained floodplains. J. Sediment. Res. 69 (4), 800–815.

Aslan, A., Autin, W.J., Blum, M.D., 2005. Causes of river avulsion: insights from the late Holocene avulsion history of the Mississippi River, USA. J. Sediment. Res. 75 (4), 650–664.

Bennett, K., 2007. Psimpoll and pscomb programs for plotting and analysis (version 4.27). Available at. http://www.chrono.qub.ac.uk/.psimpoll/psimpoll.html, Accessed date: 16 January 2016.

Birks, H.H., 2001. Plant macrofossils. In: Smol, J.P., Birks, H.J.B., Last, W.M. (Eds.), Tracking Environmental Change Using Lake Sediments. Springer, pp. 49–74.

Blaauw, M., 2010. Methods and code for 'classical'age-modelling of radiocarbon sequences. Quat. Geochronol. 5 (5), 512–518.

Blum, M.D., Toernqvist, T.E., 2000. Fluvial response to climate and sea-level change: a review and a look forward. Sedimentology 47, 2–48.

Boomer, I., von Grafenstein, U., Guichard, F., Bieda, S., 2005. Modern and Holocene sublittoral ostracod assemblages (Crustacea) from the Caspian Sea: a unique brackish, deep-water environment. Palaeogeogr. Palaeoclimatol. Palaeoecol. 225 (1), 173–186.

Butcher, S.W., 1990. The nickpoint concept and its implications regarding onlap to the stratigraphic record. In: Quantitative Dynamic Stratigraphy, pp. 375–385.

Chakraborty, T., Kar, R., Ghosh, P., Basu, S., 2010. Kosi megafan: historical records, geomorphology and the recent avulsion of the Kosi River. Quat. Int. 227 (2), 143–160.

Dolotov, Y., Kaplin, P., 2005. Black and Caspian Seas, coastal ecology and geomorphology. In: Schwartz, M.L. (Ed.), Encyclopedia of Coastal Science. Springer, pp. 194–203.

Folk, R.L., 1974. Petrology of Sedimentary Rocks. Hemphill Publishing Company, Austin, TX.

Geological maps and sections of Persia, 1957. Edward Stanford Ltd., London.

Haghani, S., Leroy, S., 2016. Differential impact of long-shore currents on coastal geomorphology development in the context of rapid sea level changes: the case of the Old Sefidrud (Caspian Sea). Quat. Int. 408, 78–92.

Haghani, S., Leroy, S.A.G., Khdir, S., Kabiri, K., Beni, A.N., Lahijani, H.A.K., 2016a. An early 'Little Ice Age' brackish water invasion along the south coast of the Caspian Sea (sediment of Langarud wetland) and its wider impacts on environment and people. Holocene 26, 3–16.

Haghani, S., Leroy, S., Wesselingh, F., Rose, N., 2016b. Rapid evolution of coastal lagoons in response to human interference under rapid sea level change: a south Caspian Sea case study. Quat. Int. 408, 93–112.

Heijst, M.V., Postma, G., 2001. Fluvial response to sea-level changes: a quantitative analogue, experimental approach. Basin Res. 13, 269–292.

Heiri, O., Lotter, A.F., Lemcke, G., 2001. Loss on ignition as a method for estimating organic and carbonate content in sediments: reproducibility and comparability of results. J. Paleolimnol. 25, 101–110.

Heyvaert, V.M.A., Baeteman, C., 2008. A middle to late holocene avulsion history of the euphrates river: a case study from tell ed-der, Iraq, lower mesopotamia. Quat. Sci. Rev. 27 (25), 2401–2410.

Hoogendoorn, R.M., Boels, J.F., Kroonenberg, S.B., Simmons, M.D., Aliyeva, E., Babazadeh, A.D., Huseynov, D., 2005. Development of the Kura delta, Azerbaijan; a record of Holocene Caspian sea level changes. Mar. Geol. 222, 359–380.

Hua, Q., Barbetti, M., Rakowski, A.Z., 2013. Atmospheric radiocarbon for the period 1950-2010. Radiocarbon 55 (4), 2059–2072.

Jones, L.S., Schumm, S.A., 2009. Causes of avulsion: an overview. In: Smith, N.D., Rogers, J. (Eds.), Fluvial Sedimentology VI. Blackwell Publishing Ltd, Oxford, UK, pp. 171–178.

Jotheri, J., Allen, M.B., Wilkinson, T.J., 2016. Holocene avulsions of the euphrates River in the najaf area of western mesopotamia: impacts on human settlement patterns. Geoarchaeology: Int. J. 31, 175–193.

Kakroodi, A.A., Kroonenberg, S.B., Goorabi, A., Yamani, M., 2013. Shoreline response to rapid 20th century sea-level change along the Iranian Caspian coast. J. Coast Res. 30 (6), 1243–1250.

Kaplin, P.A., Selivanov, A.O., 1995. Recent coastal evolution of the Caspian Sea as a natural model for coastal responses to the possible acceleration of global sea-level rise. Mar. Geol. 124, 161–175.

Kazancı, N., Gulbabazadeh, T., 2013. Sefidrud delta and quaternary evolution of the southern Caspian Lowland, Iran. Mar. Petrol. Geol. 44, 120–139.

Khabbaz-nia, A.R., Sadeghi, A., 2004. Geological Map of Rasht at 1/100 000 Scale. Sheet No. 5964. Published by Geological Survey of Iran, Tehran.

Kosarev, A.N., 2005. Physico-geographical conditions of the Caspian Sea. In: Kostianoy, A., Kosarev, A. (Eds.), The Caspian Sea Environment. Springer, Berlin, Heidelberg, pp. 5–31.

Kosarev, A.N., Kostianoy, A.G., 2005. The Caspian Sea Environment: the Handbook of Environmental Chemistry. Springer Science and Business Media.

Kousari, S., 1986. Evolution of Sefidrud delta. Development in Geological Education 1, 31–41 in Persian.

Krasnozhon, G.F., Lahijani, H., Voropayev, G.V., 1999. Evolution of the delta of the Sefidrud river, iranian Caspian Sea coast, from space imagery. Mapp. Sci. Rem. Sens. 36, 256–264.

Kroonenberg, S.B., Abdurakhmanov, G.M., Badyukova, E.N., Borg, K.V.D., Kalashinkov, A., Kasimov, N.S., Rychagov, G.I., Svitoch, A.A., Vonhof, H.B., Wesselingh, F.P., 2007. Solar-forced 2600 BP and Little Ice age highstands of the Caspian Sea. Quat. Int. 173, 137–143.

Lahijani, H.A.K., RahimpoureBonab, H., Tavakoli, V., Hosseindoost, M., 2009. Evidence for late Holocene highstands in central GuilaneEast Mazanderan, south Caspian coast, Iran. Quat. Int. 197 (1), 55–71.

Leeder, M.R., Stewart, M.D., 1996. Fluvial incision and sequence stratigraphy: alluvial responses to relative sea-level fall and their detection in the geological record. Spec. Publ. Geol. Soc. Lond. 103 (1), 25–39.

Leopold, L.B., Bull, W.B., 1979. Base level, aggradation and grade. Proc. Am. Phil. Soc. 123, 168–202.

Lepeshevkov, I.N., Buynevich, D.V., Buynevich, N.A., 1981. Perspectives of Use of Salt

Resources of Kara-bogaz-gol. Academia Nauka (in Russian), Moscow.
Leroy, S.A.G., Roiron, P., 1996. Latest pliocene pollen and leaf floras from bernasso palaeolake (escandorgue massif, hérault, France). Rev. Palaeobot. Palynol. 94 (3), 295–328.
Leroy, S.A.G., Warny, S., Lahijani, H.A.K., Piovano, E.L., Fanetti, D., Berger, A.R., 2010. The role of geosciences in the mitigation of natural disasters: five case studies. In: Beer, T. (Ed.), Geophysical Hazards. Springer, Dordrecht, pp. 115–147.
Leroy, S.A.G., Tavakoli, V., Habibi, P., Beni, M.N., Lahijani, H.A.K., Djamali, M., Naqinezhad, A., Moghadam, M.V., Arpe, K., ShaheHosseini, M., Hosseindoust, M., Miller, C.S., 2011. Late Little Ice age palaeoenvironmental records from the Anzali and Amirkola lagoons (south Caspian Sea): vegetation and sea level changes. Palaeogeogr. Palaeoclimatol. Palaeoecol. 302 (3), 415–434.
Mahmood, S., Ullah, S., 2016. Assessment of 2010 flash flood causes and associated damages in Dir Valley, Khyber Pakhtunkhwa Pakistan. Int. J. Disaster. Risk. Reduct. 16, 215–223.
Mostajeran, F., Yousefzadeh, H., Davitashvili, N., Kozlowski, G., Akbarnia, M., 2016. Phylogenetic relationships of *Pterocarya* (Juglandaceae) with an emphasis on the taxonomic status of Iranian populations using ITS and trnH-psbA sequence data. Plant Biosys.-An Int. J. Dealing with all Aspects of Plant Biol. 1–10.
Naderi Beni, A., Lahijani, H.A.K., Harami, R.M., Arpe, K., Leroy, S.A.G., Marriner, N., Berberian, M., Andrieu-Ponel, V., Djamali, M., Mahboubi, A., Reimer, P.J., 2013a. Caspian sea-level changes during the last millennium: historical and geological evidence from the south Caspian Sea. Clim. Past 9, 1645–1665.
Naderi Beni, A., Lahijani, H.A.K., Harami, R.M., Leroy, S.A.G., Shah-Hosseini, M., Kabiri, K., Tavakoli, V., 2013b. Development of spit–lagoon complexes in response to Little Ice Age rapid sea-level changes in the central Guilan coast, South Caspian Sea, Iran. Geomorphology 187, 11–26.
Ollivier, V., Fontugne, M., Lyonnet, B., Chataigner, C., 2016. Base level changes, river avulsions and Holocene human settlement dynamics in the Caspian Sea area (middle Kura valley, South Caucasus). Quat. Int. 395, 79–94.
Overeem, I., Kroonenberg, S., Veldkamp, A., Groenesteijn, K., Rusakov, G., Svitoch, A., 2003. Smallescale stratigraphy in a large ramp delta: recent and Holocene sedimentation in the Volga delta, Caspian Sea. Sediment. Geol. 159 (3), 133–157.
Posamentier, H.W., Allen, G.P., 1993. Variability of the sequence stratigraphic model: effects of local basin factors. Sediment. Geol. 86, 91–109.
Quirk, D.G., 1996. Base profile: a unifying concept in alluvial sequence stratigraphy. In: high resolution sequence stratigraphy: innovations and applications. Spec. Publ. Geol. Soc. Lond. 104, 37–49.
Reading, H.G., 2009. Sedimentary Environments: Processes, Facies and Stratigraphy. John Wiley & Sons.
Reimer, P.J., Brown, T.A., Reimer, R.W., 2004. Discussion: reporting and calibration of post-bomb 14C data. Radiocarbon 46 (3), 1299–1304.
Reimer, P.J., Bard, E., Bayliss, A., Beck, J.W., Blackwell, P.G., Ramsey, C.B., Buck, C.E., Cheng, H., Edwards, R.L., Friedrich, M., Grootes, P.M., 2013. IntCal13 and Marine13 radiocarbon age calibration curves 0–50,000 years cal BP. Radiocarbon 55, 1869–1887.
Rucevska, I., Herberlin, C., Rekacewicz, P., 2006. Vital Caspian Graphics: Challenges beyond Caviar. Arendal: UNEP/GRID.
Salter, T., 1993. Fluvial scour and incision: models for their influence on the development of realistic reservoir geometries. In: characterization of Fluvial and Aeolian Reservoirs. Spec. Publ. Geol. Soc. Lond. 73, 33–51.
Slingerland, R., Smith, N.D., 2004. River avulsions and their deposits. Annu. Rev. Earth Planet Sci. 32, 257–285.
Stouthamer, E., Berendsen, H.J.A., 2000. Factors controlling the Holocene avulsion history of the Rhine-Meuse delta (The Netherlands). J. Sediment. Res. 70 (5), 1051–1064.
Stouthamer, E., Berendsen, H.J.A., 2007. Avulsion: the relative roles of autogenic and allogenic processes. Sediment. Geol. 198, 309–325.
Stuiver, M., Reimer, P.J., 1993. Extended 14C database and revised Calib 3.0 ^{14}C age calibration program. Radiocarbon 35, 215–230.
USDA, 2016. www.pecad.fas.usda.gov/cropexplorer/global_reservoir, Accessed date: 17 June 2016.
Wang, W.M., Harley, M.M., 2004. The Miocene genus *Fupingopollenites*: comparisons with ultrastructure and pseudocolpi in modern pollen. Rev. Palaeobot. Palynol. 131, 117–145.
Wells, N.A., Dorr, J.A., 1987. Shifting of the kosi river, northern India. Geol 15, 204–207.
Wieder, M., Yaalon, D.H., 1982. Micromorphological fabrics and developmental stages of carbonate nobular forms related to soil characteristics. Geoderma 28 (3), 203–220.
Yamani, M., Moghimi, E., Motamed, A., Jafarbeglo, M., Lorestani, G., 2013. Fast shoreline changes in Sefidrud Delta using transects analyses method. Physical Geography Research Quarterly 84 (2), 1–20 in Persian.